A Protein Dynamics Study of Photosystem II: The Effects of Protein Conformation on Reaction Center Function

Sergej Vasil'ev and Doug Bruce
Department of Biological Sciences, Brock University, St. Catharines, Ontario L2S 3A1, Canada

ABSTRACT Molecular dynamics simulations have been performed to study photosystem II structure and function. Structural information obtained from simulations was combined with ab initio computations of chromophore excited states. In contrast to calculations based on the x-ray structure, the molecular-dynamics-based calculations accurately predicted the experimental absorbance spectrum. In addition, our calculations correctly assigned the energy levels of reaction-center (RC) chromophores, as well as the lowest-energy antenna chlorophyll. The primary and secondary quinone electron acceptors, Q_A and Q_B, exhibited independent changes in position over the duration of the simulation. Q_B fluctuated between two binding sites similar to the proximal and distal sites previously observed in light- and dark-adapted RC from purple bacteria. Kinetic models were used to characterize the relative influence of chromophore geometry, site energies, and electron transport rates on RC efficiency. The fluctuating energy levels of antenna chromophores had a larger impact on quantum yield than did their relative positions. Variations in electron transport rates had the most significant effect and were sufficient to explain the experimentally observed multi-component decay of excitation in photosystem II. The implications of our results are discussed in the context of competing evolutionary selection pressures for RC structure and function.

INTRODUCTION

By capturing the energy of sunlight and converting it into chemical potential energy, photosynthesis powers most life on earth. Photosynthesis occurs in a diverse range of organisms that use different kinds of photochemical reaction centers coupled to a variety of electron transport reactions. X-ray crystallographic structures and protein-sequence comparisons have shown that all known photosynthetic reaction centers share an intriguing motif of two entwined, structurally homologous polypeptides holding six chlorin chromophores between them (1–4). The reaction-center chromophores are organized into two symmetry-related branches that spread from a shared special pair of chlorins that form the primary electron donor. This common structural motif suggests a unique evolutionary origin.

Oxygenic photosynthesis uses two different reaction centers, photosystems II and I (PSII and PSI), to oxidize water and reduce $NADP^+$ to NADPH. It is the most evolutionarily successful variation of photosynthesis and the major contributor to planetary photosynthetic production. PSII is the site of water oxidation and plastoquinone reduction. As the source of planetary oxygen, PSII has had a profound impact on the evolution of life (see Barber (5) and Diner and Rappaport (6) for recent reviews on PSII).

The efficiency of oxygenic photosynthesis is enhanced by light-harvesting antenna pigments that are divided into the peripheral antenna and core antenna. The peripheral antenna systems are diverse and often variable in number, whereas the core systems are constant and more closely associated with the reaction centers. In PSI, ~100 core-antenna chlorophylls (Chls) are bound by two structurally homologous polypeptides, PsaA and PsaB, which also hold the photochemically active reaction-center chromophores (7–10). In PSII, ~30 core-antenna Chls are held by two smaller polypeptides, CP47 and CP43, which are bound to the D1 and D2 reaction-center polypeptides (11–13). Interestingly, CP47 and CP43 share some sequence homology and a folding motif with the antenna binding regions of PsaA and PsaB (3,4,7,8,10). We previously showed that 26 of the core-antenna Chls are structurally conserved between PSII and PSI (14). Of further evolutionary significance is the fact that the core-antenna binding regions of PsaA and PsaB also share a number of conserved chlorophyll liganding His residues with the ancient green sulfur bacteria and *Heliobacteria* (15,16). It is interesting that all reaction centers possessing core-antenna pigments not only share a common protein structural motif for the reaction-center chromophore-binding regions but also for the core-antenna binding regions. The conservation of this large and relatively complex protein structural motif underlines its importance in both reaction-center and core-antenna function.

X-ray structures of PSI and PSII have had a massive impact on our understanding of primary processes of photosynthesis and the structural similarities between functionally diverse reaction centers. Chromophore positions, from the x-ray structures, have provided the distance and relative orientation information required to determine pathways and efficiencies of excitation energy transfer in both PSII (17,18) and PSI (19,20). The x-ray structures of photosystems have further allowed detailed calculations of excited-state energy levels of individual antenna and reaction-center chromophores

Submitted October 7, 2005, and accepted for publication January 18, 2006.

Address reprint requests to Sergei Vasil'ev, Dept. of Biological Sciences, Brock University, St. Catharines, ON, Canada. Tel.: 905-688-5550 ext. 4163; Fax: 905-688-1855; E-mail: svassili@brocku.ca.

0006-3495/06/05/3062/12 $2.00

doi: 10.1529/biophysj.105.076075

(21) and redox potentials of electron-transport cofactors (22,23).

As x-ray structures are generated from crystallized proteins at cryogenic temperatures, they represent an average static structure. At physiological temperatures, proteins exhibit significant thermally induced fluctuations in conformation. All of the factors (distance, relative orientation, and energy levels) that affect energy transfer between photosynthetic pigments are influenced by the thermal dynamics of the proteins holding the pigments. Dynamic changes in reaction-center chromophore conformation, separation, and interaction with the protein will also influence electron-transport efficiency. How do the real-time protein dynamics of a reaction center affect the efficiency of photosynthesis?

Molecular dynamics (MD) simulations provide information concerning the thermal movements of proteins and chromophores. They offer molecular trajectories of motion that have the potential to far surpass the amount of information contained in static x-ray structures. We have applied MD simulations to the PSII core complex in its native membrane environment and generated molecular trajectories with a duration of nanoseconds. We have used the time-dependent structures as the basis for kinetic models of excited-state dynamics to see how protein dynamics affects the efficiency of energy transfer within PSII. In addition, we have done quantum mechanical (QM) calculations of the excited states of individual chromophores, based on the molecular trajectories, to determine the site energy or ''color'' of each chromophore in PSII, as well as how that color changes in time. We have also used the MD simulations of PSII to see how changes in reaction-center chromophore separation control the rate of electron transport. How accurate are the structures and dynamics that result from our molecular dynamics simulations? We found that the MD/QM simulations accurately predicted the experimental absorbance of the PSII core complex, whereas QM calculations based on the x-ray structure did not. We also found that the MD/QM calculations correctly predicted the energy levels of the chromophores with known energy levels in the PSII core. Our results have allowed us to color the PSII core chromophores and study how protein dynamics influences both structural and spectral factors that affect energy transfer and electron-transport efficiency.

METHODS

Molecular dynamics simulations

The AMBER-8 package (University of California, San Francisco, CA), the interactive molecular dynamics feature of the NAMD program (24) in conjunction with the VMD visualization program (25), and our own code have been used to set up the simulation system. For MD and energy minimization procedures we used the NAMD package (24). The simulations were performed with periodic boundary conditions in an NPT ensemble (Langevin piston coupling) at 300 K and 1 atm pressure. The long-range electrostatic interactions were calculated using the particle mesh Ewald algorithm. Both the electrostatic and the Lennard-Jones interactions had a twin-range cutoff of 8/12 Å. The multiple time step integration using an impulse-based Verlet-I method with time steps of 4 fs for long-range electrostatic forces, 2 fs for short-range nonbonded forces, and 1 fs for bonded forces was used. MD simulations were performed on the Brock Beowulf computer cluster (http://beowulf.ac.brocku.ca/beowulf/); ~10 days of central processing unit time was required for a 1-ns-long simulation using 20 computing nodes.

Force fields

The all-atom AMBER-1994 force field (26) was used for protein and the GLYCAM-2000a (27) force field for headgroups of galactolipids. For chlorophyll, pheophytin, plastoquinone, and β-carotene, we used the ab initio force field developed for the cofactors of bacterial photosynthesis (28), which was parameterized to reproduce density functional theory vibrational modes. We have modified this force field for cofactors of PSII as described below.

First we modeled the electrostatic potential field of PSII cofactors. This was accomplished by assigning partial charges to each atom. To derive atomic charges, molecular structures were first energy-minimized at a density functional level of theory with the gradient-corrected approximation of Perdew and Becke (29,30). This approximation is known to provide an accurate description of minimized geometries. To maintain consistency with the AMBER-1994 force field, we used the 6-31G* basis set. Ab initio electrostatic potential was then obtained on a set of four shells of surfaces at 1.4, 1.6, 1.8, and 2.0 times the van der Waals radii around the molecule according to a charge-fitting technique developed by the AMBER group (31). Partial atomic charges were fit to reproduce electrostatic potential on this set of grid points by a restrained electrostatic potential fit, as implemented in the RESP program from AMBER8 (UCSF, San Francisco, CA) suite. The GAUSSIAN-98 (Gaussian, Wallingford, CT) package was used for all quantum chemical calculations. Atomic charges of the oxygen evolving manganese cluster were assigned according to the redox state of its atoms in the dark-adapted (S_1) state as follows: Mn1–Mn3, +3; Mn4, +2; O1–O4, −2; Ca, +2. The atomic charge of nonheme iron was set to +2.

We then ensured that equilibrium geometries of the cofactors were accurately reproduced by the force field. Pheophytin *a* and chlorophyll *a* are only slightly different from their bacterial analogs: the imidazole ring II is unsaturated and the carbonyl group attached to ring I is replaced with a -CH group in chlorophyll *a* and pheophytin *a* This modification was accomplished by selecting proper atom types from the existing force fields. Minor modification of the plastoquinone headgroup was done using existing atom types as well. We were unable to reproduce equilibrium geometry of the conjugated double-bond system of β-carotene in a satisfactory manner using only existing atom types. To describe the equilibrium geometry of β-carotene accurately we introduced several new carbon atom types and refined force field parameters (bond lengths, angles, and dihedrals) of the bonds involving these new atom types.

Calculation of chromophore excited-state energies

Transition energies of the lowest excited state Q_Y of each chromophore were calculated ab initio using the single excitation configuration interaction (CIS) method. To account for the chromophore environment, all charges within 12 Å of any of the four Chl nitrogen atoms were included in the excited-state calculations (32,33). We used the STO-3G basis set for this calculation. This basis set is too small for accurate calculation of the absolute excited-state energies and produces excitation energies ~0.5 eV higher than experimentally determined. Nevertheless, this small basis set allowed us to complete calculations in a reasonable computation time and it has previously been shown to correctly reproduce both relative site energies and their fluctuations (32). After the CIS calculation all excited-state energies were

shifted by −0.565 eV to match the experimental room temperature peak absorbance wavelength of the PSII core complex (674 nm).

Simulation of the excited-state dynamics

A model for the light-harvesting system can be briefly described in terms of an effective Hamiltonian with diagonal elements denoting the site energies of individual chromophores and off-diagonal elements denoting the couplings between them:

$$H = \begin{pmatrix} \varepsilon_1 & H_{12} & \dots & W_{1N} \\ W_{21} & \varepsilon_2 & \dots & W_{2N} \\ \dots & \dots & \dots & \dots \\ W_{N1} & W_{N2} & \dots & \varepsilon_N \end{pmatrix},$$

where $N = 38$ for monomeric PSII.

The couplings were computed in the point dipolar approximation according to the equation:

$$W_{ij} = 5.04\mu_{eff}^2 \left(\frac{\mathbf{d}_i \cdot \mathbf{d}_j}{r_{ij}^3} - \frac{3(\mathbf{r_{ij}} \cdot \mathbf{d}_i)(\mathbf{r_{ij}} \cdot \mathbf{d}_j)}{r_{ij}^5} \right).$$

Here $\mathbf{d}_i$ denotes the unit vector along the Q_Y transition of pigment i, $\mathbf{r_{ij}}$ is a vector connecting origins of transition dipoles i and j, $\mu_{eff}^2 = 32\ D^2$ is the in situ transition dipole strength of chlorophyll a in media with a refractive index of 1.5 (34,35).

According to Förster theory, the transfer rate T_{ij} between pigments i and j can be obtained from the elements of the Hamiltonian:

$$T_{ij} = \frac{2\pi}{h}|W_{ij}|^2 J_{ij}, \quad J_{ij} = \int S_i^D(E) S_j^A(E) dE,$$

where J_{ij} is a spectral overlap between donor emission spectrum and acceptor absorption spectrum. A Stokes shift $S_i = 118\ cm^{-1}$ was calculated from the absorption spectrum of chlorophyll (36) using the Kennard-Stepanov relation to ensure detailed balance (37).

Excitation transfer rates in the system of coupled chromophores are described by the rate matrix **K** which is related to the transfer matrix **T**

$$K_{ij} = T_{ij} - \delta_{ij}(K_{PC}\delta_{i,RC} + K_{diss} + \sum_k T_{ik}).$$

To account for reversibility of the charge separation in PSII, two states representing the primary radical pair $P680^+Pheo^-$ (RP) and Q_A were added to the rate matrix **K.** The transfer rates between RP, Q_A, and the rest of the pigments were calculated as follows:

If i = RP, $K_{ij} = -\delta_{i,RC}K_{PC}$; if j = RP, $K_{ji} = -\delta_{i,RC}K_{PC}^-$; if $i = Q_A$, $K_{ij} = -\delta_{i,RP}K_{ST}$; and if j = RP, $K_{ij} = 0$.

Solution of this system of differential equations requires knowledge of the rates of several photophysical processes in PSII: charge separation between primary electron donor and Pheo, K_{PC}, its reversal K_{PC}^-, electron transfer from $Pheo^-$ to Q_A, K_{ST}, and the rate of intrinsic Chl decay by fluorescence, K_{diss}. Values of K_{ST}, K_{diss}, and K_{PC} are known from the literature. According to the experimental estimates, we used the following values of these rate constants: $K_{diss} = 0.5\ ns^{-1}$ (38), $K_{ST} = 2.5\ ns^{-1}$ (39,40), and $K_{PC} = 1000\ ns^{-1}$ (41,42), The rate of charge recombination $K_{PC}^- = 5\ ns^{-1}$ was obtained by fitting excited-state decay kinetics predicted by the model to the experimental fluorescence-decay kinetics of PSII core complex as described in Vasil'ev et al. (17,43).

The evolution of the excitation probability in time is governed by a master equation:

$$\frac{d\boldsymbol{\rho}}{dt} = -\mathbf{K} \cdot \boldsymbol{\rho}.$$

Here $\boldsymbol{\rho}$ is the vector of occupation probabilities for the excited pigments in the system and **K** is the rate matrix. This has the solution

$$\boldsymbol{\rho}(t) = \exp(-\mathbf{K}t)\boldsymbol{\rho}(0),$$

which can be expressed in terms of the matrix elements

$$\rho_i(t) = \sum_m \sum_j V_{im} \exp(-\lambda_m t) V_{mj}^{-1} \rho_E(0).$$

Here, **V** is the matrix whose columns are the eigenvectors of **K**, and λ_m is the eigenvalue of **K** associated with the column m of **V**.

Calculation of electron-transfer rates

Dutton and colleagues (44) have produced an empirical equation known as ''Dutton's Ruler'', relating electron-transfer rate to distance between cofactors:

$$Log_{10}K_{ET} = 13 - 0.6(R - 3.6) - 3.1\frac{(\Delta G + \lambda)^2}{\lambda}.$$

The initial constant 13 is the rate at van der Waals contact distance ($R = 3.6$ Å). The second term describes an approximately exponential fall-off in electron tunneling rate with distance through the insulating barrier. R is the edge-to-edge distance. The third term is the quantized Frank-Condon factor at room temperature. ΔG is free energy and λ is the reorganization energy. To obtain an optimal value of the electron-transfer rate according to Marcus theory (45) we assumed that $\Delta G = -\lambda$.

RESULTS

Preparation of the system for molecular dynamics simulation and its equilibration

The starting structure for the PSII core complex was taken from the 1S5L entry of the Protein Data Base. Protein subunits O, U, and V were removed to keep the system size at a manageable level. These extrinsic subunits are located outside the membrane, on the lumenal surface, and we assume that they do not greatly affect the structure and dynamics of PSII chromophores. Subunit N also was removed because its amino acid side chains were not identified in the x-ray structure. A disulphide bond between Cys-212(A) and Cys-211(D) was created. All histidines except His-201(B) were considered as histidines protonated at the delta position. His-201(B) was protonated at the epsilon position. Missing terminal fragments of protein chains were built using the XLEAP utility from the AMBER-8 package, and added to the system.

The x-ray structure (13) did not identify all molecules in the PSII core complex. There was a large space with unassigned electron density between the reaction center (RC) and CP43 and a smaller one between the RC and CP47. The inner surface of these cavities consists predominantly of hydrophobic atoms. Two lipid molecules are present in analogous locations between RC and antenna domains in photosystem I (9), which is structurally related to photosystem II. Most likely these cavities are occupied with aliphatic fatty acid chains of lipid molecules in PSII as well, which is why we chose to fill it with lipids. This was done interactively using

NAMD (24) and VMD (25). Eight lipid molecules were required to fill the space between CP43 and the RC and two lipid molecules were fit between CP47 and the RC. In total we used six galactolipid molecules and four phosphatidylglycerol molecules. Use of improper molecules could affect equilibrium structure and dynamics of the simulated system. Placement of the different charged groups could also affect excited states of neighboring chromophores. However, the new, higher-resolution PSII structure (2AXT entry in PDB) published after the original submission of our manuscript supports our assumption. This structure identified five lipid molecules between CP43 and the RC and two lipids between CP47 and the RC, in the same areas where we placed eight and two lipid molecules, correspondingly. There is still some unassigned electron density left in this area in the new PSII structure, consistent with the expected high disorder of the flexible fatty acid chains in the large cavity.

The whole PSII core complex was inserted into the pre-equilibrated lipid bilayer composed of monogalactosyldiacylglycerol, digalactosyldiacylglycerol, and phosphatidylglycerol with 18:3 and 16:0 fatty acids. The lipid bilayer components were chosen to represent the most abundant lipids and fatty acids found in photosystem II preparations in an approximately correct proportion (46).

The complete system, containing 573 lipids (253 monogalactosyldiacylglycerol, 160 phosphatidylglycerol, and 160 digalactosyldiacylglycerol), was neutralized by addition of 178 Na^+ ions and hydrated with 41,580 water molecules. The total number of atoms was 236,161 and the size of the system was $18 \times 16 \times 11$ nm. To start molecular dynamics simulations we first minimized the energy of the complete system. Then the temperature was gradually raised to 300 K and the system was equilibrated for 200 ps with protein and cofactors constrained to the initial positions. All atoms were then released and a second equilibration 1 ns long was carried out with constant pressure. At this stage, anisotropic pressure coupling was applied (all periodic box dimensions were allowed to fluctuate independently). After ~0.5 ns, the periodic box reached its equilibrium dimensions. All energy components remained at constant levels during the last 0.5 ns of the equilibration run, indicating that equilibrium had been reached. A snapshot of the equilibrated simulation system is shown in Fig. 1.

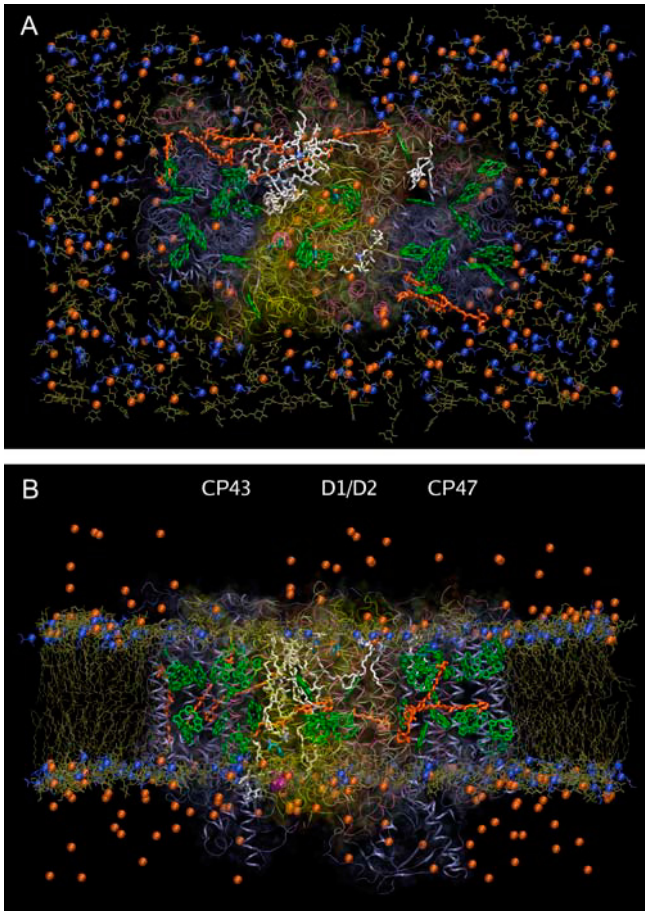

FIGURE 1 Equilibrated simulation system. (*A*) View from the stromal side of the membrane. (*B*) View along the plane of the lipid bilayer (stromal surface above). Chlorophylls are shown in green (only macrocycle atoms are shown for clarity) and β-carotene molecules are orange. Lipids filling gaps in the x-ray structure are white. Protein backbone of CP43 and CP47 is blue, backbone of D1 and D2 proteins is yellow, and other subunits are pink. Sodium and phosphate ions are orange and blue, respectively. Oxygen-evolving complex is purple.

Comparison of the equilibrated system with the x-ray structure

Our first questions were: how well did the simulated model system reproduce the reference x-ray experimental structure and how stable was the simulation in time? To address these questions we calculated the root-mean square deviation (RMSD) for the positions of all PSII chromophores. The results of this analysis are shown in Fig. 2.

RMSD was calculated using the first frame of the molecular dynamics trajectory (roughly equivalent to the x-ray structure) as a reference structure. As seen from this figure, RMSD values calculated independently for three different groups of PSII chromophores (reaction center, CP43, and CP47) were all <0.6 Å and remained constant during the entire span of the MD simulation. This indicates that the simulation was stable in time and that the molecular dynamics simulation reproduced well the experimental pigment arrangement within each of these three chromophore regions. Interestingly, the RMSD calculated for all PSII chromophores together increased significantly during the first 4–6 ns of the MD run and remained relatively constant after that. This indicates that there were slow (nanosecond) changes in the relative positions of the three chromophore-containing compartments formed by the RC (D1 and D2 polypeptides), CP47, and CP43.

Some structural reorganization of this kind is expected to occur when direct protein-protein interactions between

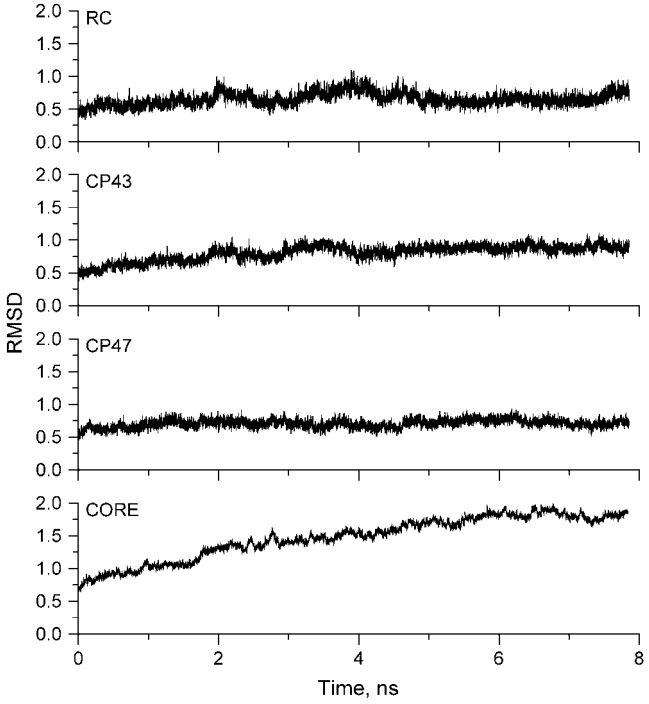

FIGURE 2 Time dependence of the root-mean-square deviations of PSII chromophore positions. The first frame of the molecular trajectory (roughly equivalent to the x-ray structure) was used as a reference. RMSD were calculated independently for three different regions in the structure, the RC (D1/D2), CP43, and CP47. RMSD was also calculated for all PSII core chromophores together, and is shown in the bottom panel.

crystallographic unit cells tightly packed in a solid phase at low temperature are replaced by protein-lipid and protein-solvent interactions at physiological temperature in a liquid phase. Thus, this reorganization may be explained by an equilibration process related to changing the protein environment from a crystal (starting point of the MD run) to a water-lipid biphasic mixture. However, we cannot exclude that it may be also related to the substitution of lipids for missing/unassigned electron densities.

Calculation of individual chromophore excitation energies and their fluctuations

Experimental studies have determined the excited-state energies of only a few PSII chromophores: Chl, coordinated by His-114 in CP47 (47), PSII RC Chls, and pheophytins (48–51). Site energy levels of the remaining antenna chromophores are difficult, if not impossible, to ascertain experimentally due to the spectral congestion arising from a large number of pigments with such similar energy levels. Theoretical assignments, based on the x-ray structure (9), have been done for PSI by semiempirical calculations of Chl excited-state energies (21). Similar work on PSII has not been feasible due to the lower resolution of the available x-ray structures (12,13).

Following the method used in Mercer et al. (32) and Damjanovic et al. (33), we calculated excited-state energies for individual chromophores in PSII using the coordinates from the x-ray structure 1S5L. This required adding protons to the structure and optimizing their positions with the molecular mechanics force field. Site energies were then calculated using the CIS excited-state calculation as described in Methods. Most of the off-diagonal elements of the system Hamiltonian were $<100\ cm^{-1}$; only three were within 100–160 cm^{-1}. This is less than the experimentally determined homogeneous chlorophyll linewidth (160–180 cm^{-1}) (36,52). Thus, the absorption spectrum of PSII can be well approximated by consideration of only diagonal elements of the Hamiltonian. Based on these findings we modeled the inhomogeneously broadened experimental absorption spectrum as a sum of Gaussians 170 cm^{-1} wide. The resulting spectrum is shown in Fig. 3. As seen from the figure, the spectrum calculated from the x-ray coordinates failed to reproduce the experimental spectrum and had a much broader bandwidth.

To calculate the PSII absorption spectrum using coordinates refined by our molecular dynamics simulation, changes of the atomic coordinates due to thermal motion must be accounted for. We found the dynamics of the system to cause strong variations of energy levels in time. Fluctuations occurring on the timescale of interaction of the chromophore with the electric field of a photon (typically <1 ps) led to broadening of its homogeneous absorption line. From time series of energy gap fluctuations, autocorrelation $C(t)$ and spectral densities $I(w)$ were obtained. From these quantities we observed that the period of the fastest energy level fluctuation was $\sim$20 fs (data not shown). Similar high-frequency modes were observed previously for both Chl in solution (32) and BChl in light-harvesting protein (33). Most probably, this mode arises from intramolecular vibration.

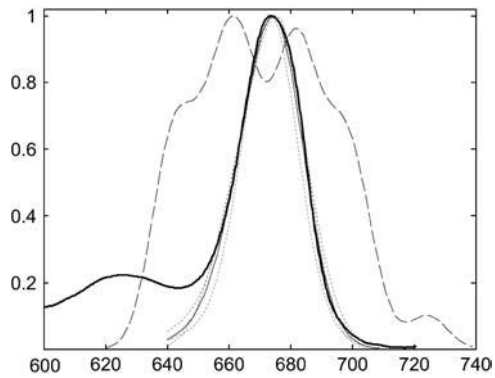

FIGURE 3 Experimental (*thick solid line*) and simulated absorbance spectra of the PSII core complex. See Methods for details on the quantum mechanical spectral simulations. The spectrum simulated using the x-ray coordinates from 1S5L is shown by the long dashed line. Spectra simulated using four different frames from the MD trajectory, separated by 1 ns, are shown by the dotted lines. The thin solid black line represents the average of the four MD simulated spectra.

Autocorrelation of energy-gap fluctuations is the key quantity allowing calculation of the absorption lineshape without artificial parameters. However, for convergence of absorption spectra, about twice as many quantum chemical computations of the excited state for each chromophore would be necessary (30). This number of computations was beyond our current computing resources. In our study, we simplified calculation of the absorption lineshape and used the same procedure described above for calculation of the absorption spectrum of the x-ray structure: we dressed Q_Y states of individual chromophores by Gaussians of the proper width and summed them up. Due to fast fluctuations, single-point calculations of the energy level from one frame of the molecular trajectory do not provide meaningful information about site energy level. To obtain mean site energy levels we calculated an average of 240 single-point excited-state calculations done with a time increment of 5 fs. We found this number and time interval of calculations to be sufficient for convergence of the mean site energy levels (data not shown).

Fluctuations occurring on longer timescales cause variation of the peak positions of individual chromophores. To characterize the amount of inhomogeneous line broadening caused by these slower motions of the pigment-lipid-protein complex we repeated our mean site energy level calculations for four different times from the molecular dynamics trajectory, each separated by 1 ns. The resulting calculated absorption spectra of the PSII core complex are shown in Fig. 3. Despite the relatively large excited-state energy fluctuations of the contributing individual chlorophylls, there was little variation of shape and peak positions of the overall spectra calculated from the four different times sampled from the molecular dynamics trajectory. These four spectra, and their average, reproduced well the experimental absorption spectra of the PSII core complex. In these calculations we used only one parameter: the width of the Gaussian distribution function σ representing the lineshape of a single chromophore. From the fit of the simulated spectra to the experimental PSII spectrum we found $\sigma = 168\ cm^{-1}$. This value is close to the $\sigma = 159\ cm^{-1}$ of Chl *a* in diethyl ether (36) and $\sigma = 170\ cm^{-1}$ of Chl *a* in pyridine (52). Recent theoretical modeling of experimental spectroscopic data from PSII samples estimated σ of Chl to be $180\ cm^{-1}$ (51).

Site energies for individual chromophores determined from the QM/MD calculations are shown in Fig. 4. Values are averages of those calculated at the four different time points in the MD simulation. Some chromophores exhibited larger variations between the four time slots than others. In addition, there were differences between the average site energies of the chromophores, some with higher and some with lower energies. Interestingly, the MD/QM calculation of excited states correctly predicted the average site energy levels of a number of PSII chromophores whose energies have been determined experimentally (see Discussion for details).

Effects of protein dynamics on energy transfer efficiency

Our MD simulations showed fluctuations in chromophore orientations, interchromophore distances, and energy levels. How do these changes influence the efficiency of excitation energy transfer from the antenna to the reaction center and thus the quantum yield of photochemistry in photosystem II?

The antenna chlorophylls of CP43 and CP47 are separated from the reaction center core chromophores by ~20 Å. At this distance, the rate of energy transfer from the antenna to the reaction center to some extent limits the overall rate of excited-state decay (18,43). The distance fluctuations between the antenna and the reaction center pigments are therefore expected to affect the experimentally observable fluorescence-decay kinetics. We analyzed fluctuations of distances between the geometrical centers of the reaction center pheophytins and their nearest antenna pigment neighbors. We

	1S5L CP43	1S5L. CP47
1	3	4
2	5	6
3	7	8
4	9	10
5		
6	11	23
7	12	26
8	13	24
9	14	31
10	15	25
11	16	29
12	17	30
13	18	28
14	19	34
15	20	35
16	21	37
17	22	36
18	44	32
19		
20	47	
21		33
22		46
23		27

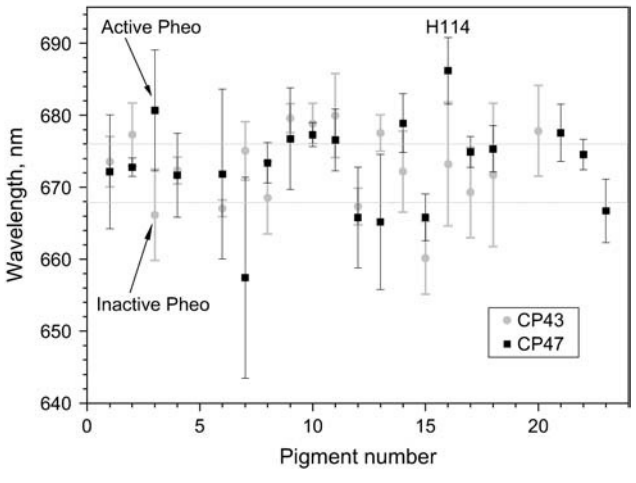

FIGURE 4 Energy levels of the Q_Y transitions of all PSII chromophores. The average energies obtained at four different times separated by 1 ns are shown along with the standard deviation. Chromophores are sorted by pigment number in such a way that symmetry-related chromophores in CP43 and CP47 have the same number on the *x* axis. The table on the left correlates the pigment number with the chromophore numbers from the 1S5L PDB structure file.

chose these pigments because they represent one of the major pathways of excitation energy transfer from light-harvesting antenna to the reaction center (18,43). Fluctuations of energy transfer rates in these pairs of pigments will have the largest impact on the efficiency and excited state lifetime of the PSII core complex. The time dependence of these fluctuations is shown in Fig. 5. As seen from this figure, the magnitudes of distance fluctuations were 2.5 Å and 2.1 Å for the CP43 and CP47 sides of the PSII core complex, respectively. The distance between the D1 pheophytin and the bridging antenna Chl in CP43 is slightly larger and more variable than the distance between the D2 pheophytin and the bridging Chl on the CP47 side. Due to the $1/R^6$ dependence of excitation-energy transfer rate on distance, the distance fluctuations we observed resulted in a factor of 2 change of excitation-energy transfer rate. It is interesting to estimate how variation of the excitation transfer rates will affect the lifetime of the system along the molecular dynamics trajectory. To achieve this, we recomputed the off-diagonal entries of the Hamiltonian for each frame of the trajectory. Diagonal entries of the Hamiltonian were kept constant. This approach is expected to account for most of the fluctuations in excitation transfer, as the latter is dominated by the dipole-dipole couplings. However, excitation transfer is not completely insensitive to the fluctuations of the diagonal elements. Future refinement of the excited dynamics involving recomputation of energy levels along the molecular dynamics trajectory will characterize contribution of the diagonal elements to the overall lifetime variation. Lifetime calculations revealed significant variations in the calculated PSII fluorescence-decay lifetimes, Fig. 5 *B*. Along with the fast distance fluctuations, caused by the vibrational modes of the chromophores (picosecond time domain), slow distance changes (nanoseconds) arising from long-range motions of the whole system are clearly seen in this figure.

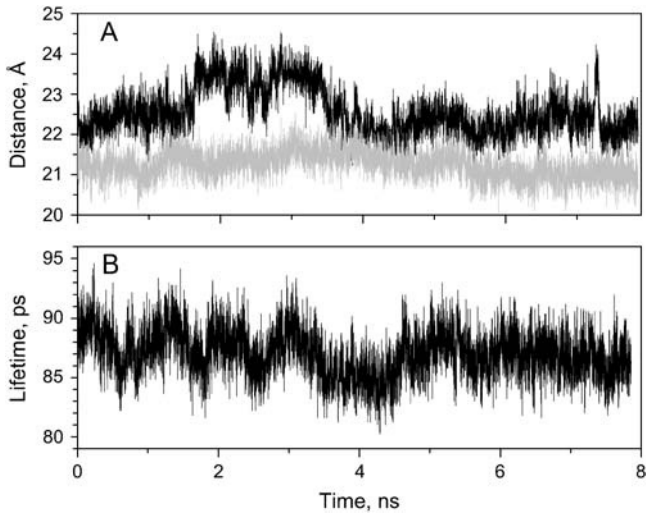

FIGURE 5 Time dependence of chromophore separation distances and mean excited-state lifetime of the PSII core complex. (*A*) Distance between CP43 Chl_{14} and D1 Pheo (*black line*) and the distance between CP47 Chl_{31} and D2 Pheo (*gray line*). (*B*) Calculated mean excited-state lifetime (see Methods for details).

Effect of protein dynamics on electron-transfer rates

Our MD simulation showed significant fluctuations in the distance between reaction center cofactors involved in photochemistry. Fig. 6 compares two representative conformations of the PSII core, from the MD simulation, focusing on the Q_A (*left panel*) and Q_B (*right panel*) binding sites. The view of Q_A includes the redox active pheophytin as well as a few of the amino acid side chains close to Q_A. The two conformations show relatively large movements of Q_A and some of the associated side chains that result in fluctuations in the distance between pheophytin and Q_A. Distance changes of this magnitude would be expected to have a significant effect on electron transport rate.

We obtained the time dependence of the edge-to-edge distance between the closest points of the conjugate systems of the chromophores from the molecular dynamics trajectory. Using the ''Dutton ruler'' we then calculated the time dependence of the electron-transfer rates from Pheo to Q_A and from Q_A to Q_B, which are shown in Fig. 7, *A* and *C*. The average calculated rate of Pheo to Q_A electron-transfer rate was 6 ns^{-1}, which is close to the experimental values of 2–5 ns^{-1} (39,53,54), indicating that the rate of this electron transport step is close to optimal. The molecular dynamics, however, revealed strong fluctuations of the rate of this electron-transfer step. At certain times, the two electron-transfer cofactors come so close to each other that the rate of electron transfer increased by a factor of 10 from its average value Fig. 7 *B*. The lowest and highest limits for K_{ET} observed during the 8-ns simulation run were 0.9 ns^{-1} and 53 ns^{-1}. The thermal dynamics of the PSII core complex modulates the rate of electron transfer such that periods with a high

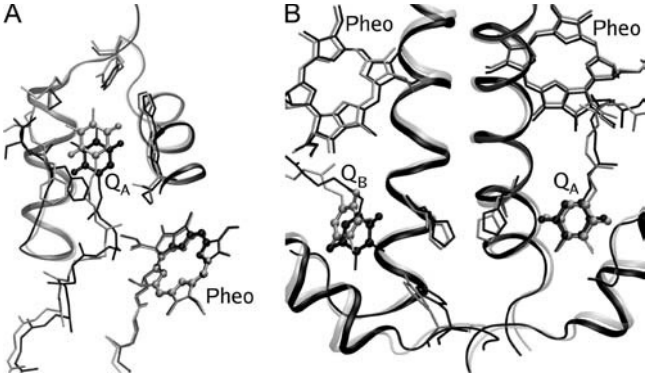

FIGURE 6 Two representative conformations of the PSII core, taken from the MD simulation, showing fluctuations in the distances between electron-transfer cofactors. (*A*) Variation of the distance between Q_A and Pheo. (*B*) Variation of the distance between Q_A and Q_B.

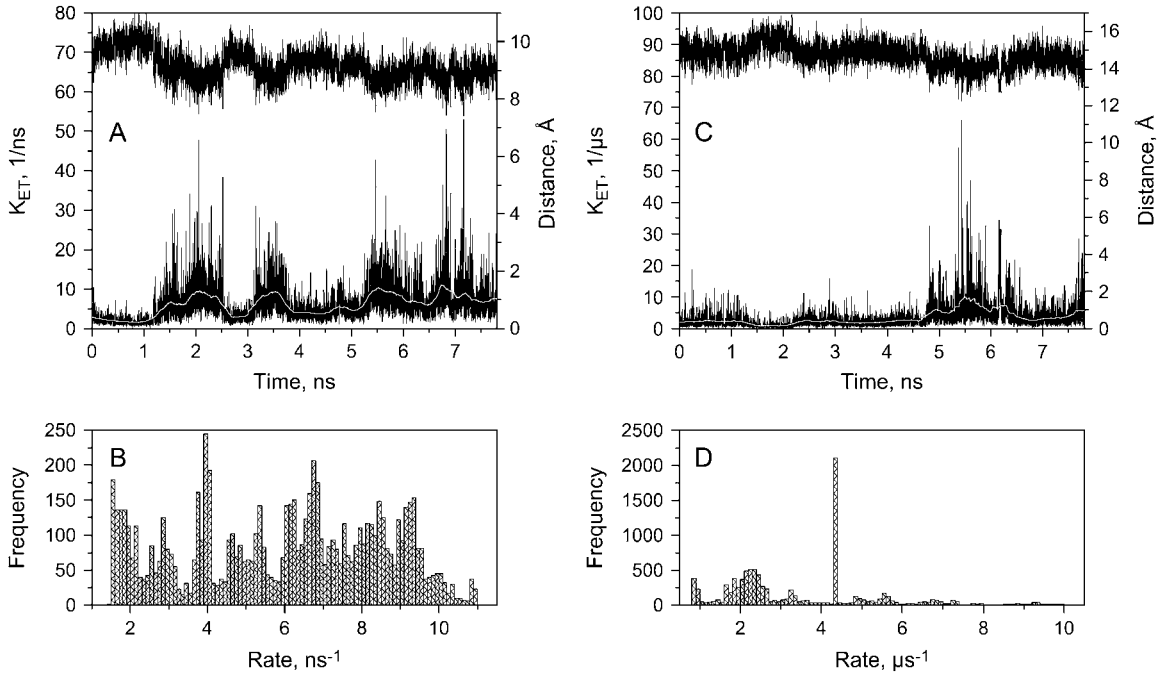

FIGURE 7 Time dependences of the edge-to-edge distance between electron-transfer cofactors. (*A*) Fluctuating distance between Pheo D1 and Q_A (*upper trace*) and the calculated rate of electron transfer between them (*lower trace*). The average rate was 6 ns^{-1}. (*B*) Histogram of the rate distribution determined from the rates presented in *A*. (*C*) Time dependence of the edge-to-edge distance between Q_A and Q_B (*upper trace*) and the calculated rate of electron transfer between them (*lower trace*). The average rate was 3.5 μs^{-1}. (*D*) Histogram of the rate distribution determined from the rates presented in *C*. The rates of electron transfer were calculated using ''Dutton's ruler'', as described in Methods.

average electron-transfer rate (8–10 ns^{-1}) are alternating with periods with a low rate (1.5–2 ns^{-1}). The system spends approximately equal time in conformations with slow and fast electron-transfer rate. The resulting distribution of K_{ET} (Fig. 7 *B*) does not resemble a bell-shaped curve; it has several different peaks, which is why the time averaged $Pheo^-$ oxidation kinetics are expected to be multi-phasic.

The calculated average optimal rate of Q_A-to-Q_B transfer was 3.5 μs^{-1}. It is faster than the experimentally determined rate of Q_A^- oxidation (55). Similar differences between optimal and experimental rates of the Q_A-to-Q_B electron-transfer step have been observed in purple bacteria (44). This difference is most likely explained by reorganization energy associated with this process. The protein dynamics modulates the rate of this electron-transfer step as well as the rate of $Pheo^-$ oxidation. However, the modulation pattern is quite different in the case of Q_A-to-Q_B transfer. Most of the time, the system is found in a conformation with Q_B in a distal position, characterized by a slow electron-transfer rate.

Implications of protein dynamics calculations on quantum efficiency

To assess how dynamic changes in chromophore geometry influence energy-transfer efficiency and thus affect the quantum yield of photochemistry in PSII, we used kinetic models for excitation energy transfer based on each of the structural configurations resulting from the MD simulation. Quantum yield was determined as the yield of reduced quinone electron acceptors in the kinetic models. Interestingly, the distribution of quantum yields resulting from changes in antenna configuration was very narrow (only 0.25%, data not shown). We found that site-energy fluctuations affected the quantum yield much more than the orientation fluctuations. The quantum yield calculated for systems with the spectral assignments determined for the four different times from the MD simulation as described above ranged from 89% to 93%. An even larger difference of 8% was found when the locations of the spectral forms were randomly shuffled in the PSII core complex (data not shown).

The electron-transfer rate from $Pheo^-$ to Q_A (K_{ST}) is critical for a high yield of photochemistry. With the parameters used in our kinetic model, fluctuations of the K_{ST} lead to a variation of quantum yield within 2%. This is a very conservative estimate, based on the optimal theoretical rate of K_{ST}. With the parameters used for the kinetic model in this study, the quantum yield reached its maximal value when K_{ST} was ~2 ns^{-1}; any further increase of K_{ST} did not improve the quantum yield. Our calculations showed that if K_{ST} was scaled down by a factor of 0.5 to bring the average K_{ST} in the kinetic model to the average of experimentally determined values, the width of the quantum yield distribution increased by a factor of 2.5 and became 5%. This is the full spread of the distribution and it does not mean that the

average yield of PSII becomes significantly lower. The average yield only goes down from 96% (for K_{ST} determined by Dutton's ruler) to 95% (for K_{ST} scaled by 0.5 to match the average experimental rate).

Effect of the dynamic changes in energy and electron transport on experimental observables

Processes of energy transfer and electron transport contribute to the decay kinetics of the excited state, which can be observed by time-resolved fluorescence and absorption experiments. Experimental fluorescence-decay kinetics of the PSII core complex are multi-exponential (17,56,57). To date, the nature of excited-state decay complexity has not been fully understood. The radical-pair equilibrium model (39,58) predicts two exponential kinetics where the second decay component arises from recombination of the primary radical pair. It has been suggested that a complex charge stabilization process is responsible for multi-exponential decay kinetics (17,59). However, excited-state decay will be affected by the molecular dynamics of the system as chromophore positions, transition dipole orientations, site energy levels, and electron-transfer rates are dynamically changing. To what extent does thermal disorder modulate excitation decay kinetics? To address this question, we calculated the fluctuation of the mean fluorescence lifetime during the time course of the MD simulation.

At first we studied how the excited-state decay depends upon position and orientation of the antenna chlorophylls. To accomplish this, we extracted positions and dipole directions of all chromophores from every snapshot of the atomic trajectory saved every picosecond of the MD. Using this data we calculated fluctuations in the excitation lifetime. Only the distance and orientation factors in the Förster equation were changed in this case. The time dependence of the excitation lifetime is shown in Fig. 5 *B*. As seen from this figure, increases in distances between the linkers and the reaction center were correlated with longer excitation lifetimes. We observed changes of ~15% in the lifetime during the time course of our simulation. However, the average fluorescence-decay kinetics, obtained by averaging the individual kinetics calculated for each snapshot of the atomic trajectory, was well described by two exponential decay phases and was indistinguishable from fluorescence-decay kinetics calculated from the original x-ray configuration of chromophores. Thus, we conclude that variations of the decay kinetics caused by positional and orientational disorder did not result in the appearance of new fluorescence-decay components.

We then studied how excited-state dynamics are modulated by fluctuations of electron-transfer rate. The rate of electron transfer from Pheo to Q_A defines the lifetime of the slow component of the excited-state decay. We therefore expect a large degree of fluorescence-decay inhomogeneity (appearance of several slow fluorescence-decay components with different lifetimes) to arise due to thermal fluctuation of the distance between Pheo and Q_A. Indeed, when we calculated the average fluorescence-decay kinetics using time-dependent K_{ST} resulting from the molecular dynamics simulation we found that four decay components (77% 64 ps, 17.5% 140 ps, 4% 300 ps, and 1.5% 614 ps) were required to describe fluorescence decay. Two additional slow-decay components appeared in the excited-state decay kinetics due to the fluctuation of the rate of electron transfer. These components are similar to the experimentally observable slow fluorescence-decay components (17,60). For this calculation we used the optimal K_{ST}. Even more complex fluorescence-decay kinetics were found when we scaled K_{ST} down to bring the average K_{ST} to the average of experimentally determined values as described above.

DISCUSSION

During the timescale of the MD simulation we observed a rearrangement of the polypeptides, revealed by RMSD deviation calculations for individual chromophore positions. Chromophore positions within individual pigment-binding polypeptides were relatively constant compared to those calculated for the entire protein complex. This is consistent with positional rearrangements of the CP47 and CP43 subunits with respect to the D1/D2 reaction center core subunits. The subunit position changes likely reflect a conformation shift as the starting conformation (from the crystal structure) of the PSII core complex equilibrated with the lipid bilayer. It is interesting that the positions of the reaction center chromophores showed no larger changes in RMSD than did the chromophores bound within either of the two core-antenna polypeptides (CP43 and CP47), even though the reaction-center chromophores have ligands from two separate polypeptides (D1 and D2). This is consistent with the relatively strong connections between the D1 and D2 polypeptides, which are wrapped around each other, have ligands to the nonheme iron, and are covalently attached by a disulphide bridge between Cys-212/D1 and Cys-211/D2. CP47 and CP43 are more loosely associated with the central D1/D2 complex. Our measurements of distance fluctuations between the pheophytins of the D1/D2 complex and the linker chlorophylls of CP43 and CP47 clearly show a greater variation for CP43 than for CP47. This is consistent with the experimentally observed weaker binding of CP43 to the PSII core complex as compared to the more tightly bound CP47.

Fluctuations in chromophore geometry arising from the dynamical motions of their polypeptide ligands were found to contribute relatively little to variation in the efficiency of energy transfer and calculated quantum yield as determined with kinetic models. The PSII antenna system is robust and delivers virtually the same high efficiency despite relatively large fluctuations of energy transfer rates from linker Chls to the core. More variation in energy-trapping efficiency was introduced by variations in the excited-state energy levels of the antenna resulting from changing chromophore conformations

and changing chromophore protein and/or solvent interactions. Individual chromophores showed a range of excited-state energy variations. Due to high computational cost, we were able to perform excited-state calculations only for the system at four different times during the molecular trajectory. This was not sufficient to observe the full extent of variation in excited-state site energies. Thus, our data represent a conservative estimate of variation in energy-trapping efficiency.

The absorption spectrum of Chl is clearly broadened by its interaction with protein ligands. This is most likely driven by a strong selection pressure to increase the distribution of antenna chromophore energy levels to increase the effective light-harvesting capability of the reaction center. Protein-induced antenna spectral broadening has often been presumed to arise predominantly from variations in individual chromophore site energies which arise from site-dependent differences in protein-chromophore interactions. Our MD simulation shows that variation in the overall distribution of antenna chromophore energy levels originates dynamically within individual sites as well as between different sites. Protein dynamics thus plays a significant role in increasing the bandwidth of Chl absorption.

Our calculations have correctly reproduced the absorption spectrum of the PSII core complex, confirmed the site energy levels of the RC chromophores recently derived analytically (51), and correctly identified the lowest-energy Chl in PSII (61). These results lend strong support to our MD/QM calculated assignments for the site energies of each individual PSII antenna chromophore. Our simulation identifies the lowest-energy chlorophyll in PSII as Chl coordinated by CP47 His-114. This is the same Chl that was found experimentally, by site-directed mutagenesis (61), to be the source of the long-wavelength fluorescence emission (695 nm) in PSII. Our calculations place the excited state of active (D1) pheophytin higher than the inactive (D2) pheophytin. At first glance, this is in contradiction to experimental assignments that have been made based upon spectroscopic changes induced by reduction of Pheo and/or Q_A. In that work, the energy levels of the D1/D2 pheophytins were found to lie at 681/670–672 nm (48) in isolated PSII reaction centers, at 685.6/669.3 nm in PSII core complexes of cyanobacteria *Synechocystis* (49), and at 685.3/670 nm in plant PSII core complexes (50). However, recent detailed calculations of PSII reaction-center optical properties based on its x-ray structure have shown that the site energy of D1 Pheo should actually be higher than the energy of the D2 Pheo to account for a wealth of spectroscopic data (51). These calculations place the D1 Pheo energy at 672 nm. The authors attribute the discrepancy in data interpretation to a mixture of excitonic and electrochromic effects that result in a bleaching at 681–685 nm upon reduction of D1 Pheo even though its site energy is at 672 nm (51). The results of our study are in agreement with the latter identification of site energies of pheophytins, as well as all other PSII RC chromophores (Table 1). Our results also confirmed similar site energies for both P680 monomers and ChlZ/D. The higher site energy for the accessory Chl D1 compared to its D2 analog was also reproduced.

Bacterial reaction centers and PSII belong to the Type II group of reaction centers and are characterized by having two quinone electron acceptors. The x-ray structures of dark-adapted and light-adapted bacterial RC from *Rhodobacter sphaeroides* have been solved, and analysis of the Q_A and Q_B binding pockets revealed two binding sites for Q_B: a distal binding site in the dark-adapted x-ray structure and a proximal binding site in the light-adapted structure (62,63). The conformational change observed in bacterial RC x-ray structures is similar to the conformational change between two Q_B binding-site conformations that emerged in our MD simulation of the PSII reaction-center core (Fig. 6). The headgroup of Q_B was displaced in the same direction and the aliphatic tail exhibited the same propeller-like motion observed in the bacterial x-ray structures. In our simulation, the system was in the state equivalent to the dark-adapted state (no charge on Q_A). We found Q_B to be in the distal binding pocket most of the time, corresponding to the dark-adapted bacterial reaction-center structure and only ~10% of the time in the state resembling the light-adapted x-ray conformation. Compared to the conformation of the light-adapted bacterial x-ray structure, the proximal Q_B conformation observed in our MD simulation was intermediate between the light-adapted and dark-adapted x-ray structures. These findings strongly suggest the possibility of a light-induced conformational gating in the PSII reaction center, which may be a common feature for Type II photosynthetic reaction centers.

Our MD study has revealed relationships between protein dynamics, the configuration of the light-harvesting antenna system, and electronic properties of chromophores in the PSII core complex. This information, combined with kinetic modeling of the photochemical reactions, has allowed us to quantify the contribution of different dynamic changes to the efficiency of primary photosynthetic energy conversion. Our MD calculations thus offer novel insight into the evolution of a variety of processes, operating at a number of different levels that contribute to the photochemical efficiency of PSII. Selection pressures operating on a variety of parameters, sometimes in competition with each other, must be considered when looking at the optimization of reaction-center efficiency. For example, although efficient light harvesting

TABLE 1 Assignment of the site energies of PSII reaction-center chromophores

Chromophore	D1	D2
P680	672 (666)	672 (666)
Acc Chl	677 (678)	673 (667)
Pheo	666 (672)	681 (675)
ChlZ	672 (667)	672 (667)

The published values taken from Raszewski (51) are given in parentheses for comparison with our calculations.

requires a dense packing of chromophores, a minimum separation must be maintained to prevent aggregation and formation of quenching centers. Evolutionary solutions to this dilemma appear limited, as all reaction centers containing core-antenna chromophores share a homologous antenna binding polypeptide motif. We have previously shown that this common chromophore binding motif results in the majority of PSII antenna chromophores having highly positionally conserved counterparts in PSI (14). Interestingly, not all of these conserved chromophores are orientationally optimized for energy transfer. Clearly, other selection pressures are operating and other factors (i.e., protein folding constraints related to maximizing pigment density and minimizing the formation of quenching centers) are involved. Our MD/QM calculations of chromophore site energies show that protein-chromophore interactions influence the absorption of light by antenna chromophores. Protein dynamics increase the effective absorption bandwidth of all individual chromophores. From an evolutionary point of view, this will confer an advantage by increasing the potential of the antenna to capture light. In addition, individual sites have different average peak wavelengths, which means the localization of spectral forms must be considered when assessing photosynthetic efficiency. The localization and extent of dynamic variation of individual chromophore spectra will strongly influence the efficiency of light energy transfer from core antenna to the reaction center, between other auxiliary antenna systems and the core antenna, between monomers in PSII dimers, and even between PSII and PSI. This competing array of selection pressures still does not include explicit consideration of any of the photoregulatory mechanisms known to affect light harvesting by PSII. The most significant effect on photosynthetic efficiency we observed in our MD calculations arose from the movements of the two quinone electron acceptors, Q_A and Q_B. The positional changes we observed in Q_B compared to those previously observed between dark-adapted and light-adapted bacterial reaction centers suggests that conformational changes affecting electron transport efficiency triggered by light may be a common factor in Type II reaction centers (62). In summary, our MD calculations show a strong influence of protein dynamics on energy transfer and electron-transport efficiency in the PSII core. Our work also provides an additional framework for understanding the evolution of photosynthetic reaction centers and underlines the importance of considering protein dynamics in reaction-center structure and function.

The authors gratefully acknowledge the support of Discovery and Equipment grants from the Natural Science and Engineering Research Council of Canada

REFERENCES

1. Michel, H., and J. Deisenhofer. 1988. Relevance of the photosynthetic reaction center from purple bacteria to the structure of photosystem II. *Biochemistry*. 27:1–7.
2. Barber, J., and B. Andersson. 1994. Revealing the blueprint of photosynthesis. *Nature*. 370:31–34.
3. Rhee, K. H., E. P. Morris, J. Barber, and W. Kuhlbrandt. 1998. Three-dimensional structure of the plant photosystem II reaction centre at 8 Å resolution. *Nature*. 396:283–286.
4. Schubert, W.-D., O. Klukas, W. Saenger, H.-T. Witt, P. Fromme, and N. Krauß. 1998. A common ancestor for oxygenic and anoxygenic photosynthetic systems: a comparison based on the structural model pf photosystem I. *J. Mol. Biol.* 280:297–314.
5. Barber, J. 2003. Photosystem II: the engine of life. *Q. Rev. Biophys.* 36:71–89.
6. Diner, B. A., and F. Rappaport. 2003. Structure, dynamics, and energetics of the primary photochemistry of photosystem II of oxygenic photosynthesis. *Annu. Rev. Plant Biol.* 53:551–580.
7. Krauß, N., W.-D. Schubert, O. Klukas, P. Fromme, H.-T. Witt, and W. Saenger. 1996. Photosystem I at 4 Å resolution represents the first structural model of a joint photosynthetic reaction centre and core antenna system. *Nat. Struct. Biol.* 3:965–973.
8. Klukas, O., W.-D. Schubert, P. Jordan, N. Krauß, P. Fromme, H.-T. Witt, and W. Saenger. 1999. Photosytem I, an improved model of the stromal subunits PsaC, PsaD, and PsaE. *J. Biol. Chem.* 274:7351–7360.
9. Jordan, P., P. Fromme, H.-T. Witt, O. Klukas, W. Saenger, and N. Krauß. 2001. Three-dimensional structure of cyanobacterial photosystem I at 2.5 Å resolution. *Nature*. 411:909–917.
10. Ben Shem, A., F. Frolow, and N. Nelson. 2003. Crystal structure of plant photosystem I. *Nature*. 426:630–635.
11. Zouni, A., H.-T. Witt, J. Kern, P. Fromme, N. Krauß, W. Saenger, and P. Orth. 2001. Crystal structure of oxygen evolving photosystem II from *Synechococcus elongatus* at 3.8 Å resolution. *Nature*. 409:739–743.
12. Kamiya, N., and J.-R. Shen. 2003. Crystal structure of oxygen-evolving photosystem II from *Thermosynechococcus vulcanus at* 3.7-Å resolution. *Proc. Natl. Acad. Sci. USA*. 100:98–103.
13. Ferreira, K. N., T. M. Iverson, K. Maghlaoui, J. Barber, and S. Iwata. 2004. Architecture of the photosynthetic oxygen-evolving center. *Science*. 303:1831–1838.
14. Vasil'ev, S., and D. Bruce. 2004. Optimization and evolution of light harvesting in photosynthesis: the role of antenna chlorophyll conserved between photosystem II and photosystem I. *Plant Cell*. 16:3059–3068.
15. Fyfe, P. K., M. R. Jones, and P. Heathcote. 2002. Insights into the evolution of the antenna domains of Type-I and Type-II photosynthetic reaction centres through homology modelling. *FEBS Lett.* 530:117–123.
16. Heathcote, P., P. K. Fyfe, and M. R. Jones. 2002. Reaction centres: the structure and evolution of biological solar power. *Trends Biochem. Sci.* 27:79–87.
17. Vasil'ev, S., C.-I. Lee, G. W. Brudvig, and D. Bruce. 2002. Structure-based kinetic modeling of excited-state transfer and trapping in His-tagged PSII core complexes from *Synechocystis*. *Biochemistry*. 41: 12236–12243.
18. Vasil'ev, S., J.-R. Shen, N. Kamiya, and D. Bruce. 2004. The orientations of core antenna chlorophylls in photosystem II are optimized to maximize the quantum yield of photosynthesis. *FEBS Lett.* 561:111–116.
19. Sener, M. K., D. Y. Lu, T. Ritz, S. Park, P. Fromme, and K. Schulten. 2002. Robustness and optimality of light harvesting in cyanobacterial photosystem I. *J. Phys. Chem. B*. 106:7948–7960.
20. Byrdin, M., P. Jordan, N. Krauss, P. Fromme, D. Stehlik, and E. Schlodder. 2002. Light harvesting in photosystem I: Modeling based on the 2.5-angstrom structure of photosystem I from *Synechococcus elongatus*. *Biophys. J.* 83:433–457.
21. Damjanovic, A., H. M. Vaswani, G. R. Fleming, and P. Fromme. 2002. Chlorophyll excitations in Photosystem I of *Synechoccus elongatus*. *J. Phys. Chem. B*. 106:10251–10262.
22. Hasegawa, K., and T. Noguchi. 2005. Density functional theory calculations on the dielectric constant dependence of the oxidation potential of chlorophyll: implication for the high potential of P680 in photosystem II. *Biochemistry*. 44:8865–8872.

23. Ishikita, H., B. Loll, J. Biesiadka, W. Saenger, and E. W. Knapp. 2005. Redox potentials of chlorophylls in the photosystem II reaction center. *Biochemistry*. 44:4118–4124.
24. Kale, L., R. Skeel, M. Bhandarkar, R. Brunner, A. Gursoy, N. Krawetz, J. Phillips, A. Shinozaki, K. Varadarajan, and K. Schulten. 1999. NAMD2: greater scalability for parallel molecular dynamics. *J. Comput. Phys.* 151: 283–312.
25. Humphrey, W., A. Dalke, and K. Schulten. 1996. VMD: visual molecular dynamics. *J. Mol. Graph.* 14:33–38.
26. Cornell, W. D., P. Cieplak, C. I. Bayly, I. R. Gould, K. M. Merz, D. M. Ferguson, D. C. Spellmeyer, T. Fox, J. W. Caldwell, and P. A. Kollman. 1995. A second generation force field for the simulation of proteins, nucleic acids, and organic molecules. *J. Am. Chem. Soc.* 117:5179–5197.
27. Basma, M., S. Sundara, D. Calgan, T. Vernali, and R. J. Woods. 2001. Solvated ensemble averaging in the calculation of partial atomic charges. *J. Comput. Chem.* 22:1125–1137.
28. Ceccarelli, M., P. Procacci, and M. Marchi. 2003. An ab initio force field for the cofactors of bacterial photosynthesis. *J. Comput. Chem.* 24:129–142.
29. Perdew, J. P. 1986. Density-functional approximation for the correlation-energy of the iInhomogeneous electron-gas. *Phys. Rev. B.* 33:8822–8824.
30. Becke, A. D. 1986. Density functional calculations of molecular-bond energies. *J. Chem. Phys.* 84:4524–4529.
31. Bayly, C. I., P. Cieplak, W. D. Cornell, and P. A. Kollman. 1993. A well-behaved electrostatic potential based method using charge restraints for deriving atomic charges: the RESP model. *J. Phys. Chem.* 97:10269–10280.
32. Mercer, I. P., I. R. Gould, and D. Klug. 1999. A quantum mechanical/molecular mechanical approach to relaxation dynamics: calculation of the optical properties of solvated bacteriochlorophyll *a*. *J. Phys. Chem. B.* 103:7720–7727.
33. Damjanovic, A., I. Kosztin, U. Kleinekathofer, and K. Schulten. 2002. Excitons in a photosynthetic light-harvesting system: a combined molecular dynamics, quantum chemistry, and polaron model study. *Phys. Rev. E.* 65:031919.
34. Knox, R. S. 2003. Dipole and oscillator strengths of chromophores in solution. *Photochem. Photobiol.* 77:492–496.
35. Knox, R. S., and B. Q. Spring. 2003. Dipole strengths in the chlorophylls. *Photochem. Photobiol.* 77:497–501.
36. Shipman, L. L., T. M. Cotton, J. R. Norris, and J. J. Katz. 1976. An analysis of the visible absorption spectrum of chlorophyll-a monomer, dimer, and oligomers in solution. *J. Am. Chem. Soc.* 98:8222–8230.
37. Laible, P. D., R. S. Knox, and T. G. Owens. 1998. Detailed balance in Forster-Dexter excitation transfer and its application to photosynthesis. *J. Phys. Chem. B.* 102:1641–1648.
38. Roelofs, T. A., C.-H. Lee, and A. R. Holzwarth. 1992. Global target analysis of picosecond chlorophyll fluorescence kinetics from pea chloroplasts. *Biophys. J.* 61:1147–1163.
39. Schatz, G. H., H. Brock, and A. R. Holzwarth. 1988. Kinetic and energetic model for the primary processes in photosystem II. *Biophys. J.* 54:397–405.
40. Leibl, W., J. Breton, J. Deprez, and H.-W. Trissl. 1989. Photoelectric study on the kinetics of trapping and charge stabilization in oriented PSII membranes. *Photosynth. Res.* 22:257–275.
41. Gobets, B., I. H. M. van Stokkum, F. van Mourik, J. P. Dekker, and R. van Grondelle. 2003. Excitation wavelength dependence of the fluorescence kinetics in photosystem I particles from *Synechocystis* PCC 6803 and *Synechococcus elongatus*. *Biophys. J.* 85:3883–3898.
42. Vasil'ev, S., G. W. Brudvig, and D. Bruce. 2003. The X-ray structure of photosystem II reveals a novel electron transport pathway between P680, cytochrome b(559) and the energy-quenching cation, Chl(Z)(+). *FEBS Lett.* 543:159–163.
43. Vasil'ev, S., P. Orth, A. Zouni, T. G. Owens, and D. Bruce. 2001. Excited-state dynamics in photosystem II: insights from the x-ray crystal structure. *Proc. Natl. Acad. Sci. USA.* 98:8602–8607.
44. Moser, C. C., C. C. Page, R. Farid, and P. L. Dutton. 1995. Biological electron-transfer. *J. Bioenerg. Biomembr.* 27:263–274.
45. Marcus, R. A. 1996. Electron transfer reactions in chemistry. Theory and experiment. *In* Protein Electron Transfer. D. S. Bendall, editor. Bios Scientific, Oxford, UK.
46. Murata, N., S.-I. Higashi, and Y. Fujimura. 1990. Glycerolipids in various preparations of photosystem II from spinach chloroplasts. *Biochim. Biophys. Acta.* 1019:261–269.
47. Shen, G., J. J. Eaton-Rye, and W. Vermaas. 1993. Mutation of histidine residues in CP47 leads to destabilization of the photosystem II complex and to impairment of light energy transfer. *Biochemistry.* 32:5109–5115.
48. Jankoviac, R., M. Rästep, R. Picorel, M. Seibert, and G. J. Small. 1999. Excited states of the 5-chlorophyll photosystem II reaction center. *J. Phys. Chem.* 103:9759–9769.
49. Stewart, D. H., P. J. Nixon, B. A. Diner, and G. W. Brudvig. 2000. Assignment of the Q_y absorbance bands of Photosystem II chromophores by low-temperature optical spectroscopy of wild-type and mutant reaction centers. *Biochemistry.* 39:14583–14594.
50. Peterson, S., V. M. Masters, B. J. Prince, P. J. Smith, R. J. Pace, and E. Krausz. 2003. Optical spectra of *Synechocystis* and spinach photosystem II preparations at 1.7K: Identification of the D1-pheophytin energies and stark shifts. *J. Am. Chem. Soc.* 125:13063–13074.
51. Raszewski, G., W. Saenger, and T. Renger. 2005. Theory of optical spectra of photosystem II reaction centers: location of the triplet state and the identity of the primary electron donor. *Biophys. J.* 88:986–998.
52. Umetsu, M., Z.-Y. Wang, M. Kobayashi, and T. Nozawa. 1999. Interaction of photosynthetic pigments with various organic solvents. Magnetic circular dichroism approach an application to chlorosomes. *Biochim. Biophys. Acta.* 1410:19–31.
53. Nuijs, A. M., H. J. Van Gorkom, J. J. Plijter, and L. M. H. Duysens. 1986. Primary charge separation and excitation of chlorophyll a in photosystem II particles from spinach as studied by picosecond absorbance-difference spectroscopy. *Biochim. Biophys. Acta.* 848:167–175.
54. Eckert, H.-J., N. Wiese, J. Bernarding, H.-J. Eichler, and G. Renger. 1988. Analysis of the electron transfer from $Pheo^-$ to Q_A in PSII membrane fragments from spinach by time resolved 325 nm absorption changes in the picosecond domain. *FEBS Lett.* 240:153–158.
55. de Wijn, R., and H. J. Van Gorkom. 2001. Kinetics of electron transfer from Q_A to Q_B in photosystem II. *Biochemistry.* 40:11912–11922.
56. Andrizhiyevskaya, E. G., D. Frolov, R. van Grondelle, and J. P. Dekker. 2004. On the role of the CP47 core antenna in the energy transfer and trapping dynamics of photosystem II. *Phys. Chem. Chem. Phys.* 6:4810–4819.
57. Klug, D. R., J. R. Durrant, and J. Barber. 1998. The entanglement of excitation energy transfer and electron transfer in the reaction centre of photosystem II. *Philos. Trans. R. Soc. Lond. A.* 356:449–464.
58. Schatz, G. H., H. Brock, and A. R. Holzwarth. 1987. Picosecond kinetics of fluorescence and absorbance changes in photosystem II particles excited at low photon density. *Proc. Natl. Acad. Sci. USA.* 84:8414–8418.
59. Konermann, L., G. Gatzen, and A. R. Holzwarth. 1997. Primary processes and structure of the photosystem II reaction center. 5. Modeling of the fluorescence kinetics of the D_1-D_2-cyt-b_{559} complex at 77 K. *J. Phys. Chem.* 101:2933–2944.
60. van Mieghem, F. J. E., G. F. W. Searle, A. W. Rutherford, and T. J. Schaafsma. 1992. The influence of the double reduction of Q_A on the fluorescence decay kinetics of photosystem II. *Biochim. Biophys. Acta.* 1100:198–206.
61. Shen, G., and W. Vermaas. 1994. Mutation of chlorophyll ligands in the chlorophyll-binding CP47 protein as studied in a *Synechocystis* sp. PCC 6803 photosystem I-less background. *Biochemistry.* 33:7379–7388.
62. Rabenstein, B., G. M. Ullmann, and E. W. Knapp. 2000. Electron transfer between the quinones in the photosynthetic reaction center and its coupling to conformational changes. *Biochemistry.* 39:10487–10496.
63. Stowell, M. H. B., T. M. McPhillips, D. C. Rees, S. M. Soltis, E. Abresch, and G. Feher. 1997. Light-induced structural changes in photosynthetic reaction center: implications for mechanism of electron-proton transfer. *Science.* 276:812–816.